FOAMED GEOPOLYMERS FOR FIRE PROTECTION: BURN-THROUGH TESTING AND MODELING

Serge Bourbigot*[1,2], Johan Sarazin[1], Catherine A. Davy[3], Gaëlle Fontaine[1]

[1]Univ. Lille, CNRS, INRAE, Centrale Lille Institut, UMR 8207 - UMET - Unité Matériaux et Transformations, F-59000 Lille, France
[2]Institut Universitaire de France (IUF)
[3]Univ. Lille, CNRS, Centrale Lille Institut, Univ. Artois, UMR 8181 - UCCS - Unité de Catalyse et de Chimie du Solide, Lille F-59000, France

*Corresponding author: serge.bourbigot@centralelille.fr

Abstract

Geopolymer (GP) foam as a fire protective coating was synthesized, deposited on a steel plate, hardened and evaluated using a burn-through test at a reduced scale. It was shown that the GP foam acts as an efficient fire barrier (with 250°C reduction compared to virgin steel evaluated in the same conditions). A numerical model using Comsol Multiphysics® (finite element code) was performed to simulate the fire behavior of the GP foam. It was based on the complete characterization of the GP foam to provide accurate input data for the model. The latter captures well the temperature rise, including the endothermal effect due to water vaporization. A parametric study of the porosity and the emissivity at the surface of the GP foam brings new insights to optimize the performance of the GP foam. It is shown that a porosity of 90% and an emissivity lower than 0.75 should provide the highest performance to GP foam. The fabrication of an optimized GP foam is feasible using a technology of low emissivity thin coating and by adjusting the synthesis of the GP foam to increase its porosity.

Keywords: geopolymer, numerical simulation, modeling, fire protection, coating

Introduction

In the event of a fire in buildings, vehicles or means of transportation, the fire resistance time of the materials and products is the most critical variable and has a direct influence on the occupants' safety. Fire-resistant products should allow the structures to retain their minimum functions during the time required to evacuate the people, even despite the extreme conditions of heat and pressure to which they are subjected. A method to make structural parts fire-resistant is to use passive fire protections such as intumescent coatings[1,2]. The intumescence mechanism with polymeric coatings involves that the matrix expands as gases are produced (from the blowing agent and/or from the decomposition products of the polymeric matrix) and at the same time, cross-linking reactions and charring cause the matrix to harden, thereby producing a coherent highly porous char. The porosity of the char is generally extremely high so that the resulting structure has extremely low thermal conductivity. The most important parameters of the expanded char, affecting its thermal insulation performance, are its heat conductivity and its ability to swell. The usual chemistry of intumescence involves a polymer

composition containing an inorganic acid or a material yielding acidic species, comprising a char former and a component that decomposes to enable the expansion of the system (blowing agent).

The aim of this paper is to consider another chemistry to make intumescent coatings (foamy coatings). Aluminosilicate composites, or in other words, geopolymers (GPs) can be used to this purpose. Geopolymers are inorganic materials (cement-like) made of sodium or potassium aluminosilicates[3,4]. They exhibit high thermal stability and they can be used in harsh environments. This approach was evaluated by Schartel et al.[5] to protect steel plates according to a cellulosic fire scenario (ISO 834). Two aluminosilicate formulations were prepared based either on microsilica and alumina or on metakaolin and microsilica, containing or not flame retardants including boron trioxide, borax, aluminum trihydroxide (ATH) and magnesium dihydroxide (MDH). An intumescent behavior was observed during fire testing (with up to 300% expansion), which is an unusual behavior for geopolymers. The best fire insulation was obtained with 10% borax in the formulation based on microsilica and alumina (original layer thickness of 6 mm). The fire protection duration can reach up to 30 min (at a failure temperature of 500°C). Other geopolymers were prepared consisting of metakaolin-based alkaline aluminosilicate with a swelling agent and calcium carbonate as intumescent coating for the fire protection of structural elements[6]. An intumescent behavior was observed and the resulting material exhibits low heat conductivity and good mechanical stability. In another work[7], rice husk ash was incorporated in a metakaolin-based geopolymer to make fire resistant coating for structural insulated panel. The optimized geopolymer-based coating permits to resist 2h at the torch test before reaching 100°C. A relatively high degree of expansion was observed but some cracks and holes can be distinguished on the residues after fire testing. A foam version of GPs also exists, which is made with metakaolin and by acid- or alkali-activation[8]. The foamed GP exhibits high mechanical strength, thermal stability and fire resistance[4,9,10].

In this paper, we consider a GP foam as fire protective coating. It was evaluated on steel plate using a burn-through test at a reduced scale with a complete set of instrumentation[11]. In those conditions (burn-through fire scenario), the numerical simulation of the fire protective behavior of the GP foam was performed. The purpose was to quantify the efficiency of the GP foam as a protective coating by numerical simulation based on a comprehensive model.

Experimental

Materials

Metakaolin powder (Argical M1000, Imerys, France), silica fume (Condensil, France), commercial

sodium silicate solution (Betol 39T, Woellner, Germany) and sodium hydroxide pellets (purity of 99%, Sigma Aldrich) were used as raw materials. The presence of silica fume creates a foaming effect releasing H_2, which was enhanced by the incorporation of 2%wt hydrogen peroxide H_2O_2 (in aqueous solution at a concentration of 30%wt). A surfactant (CetylTrimethyl Ammonium Bromide, $CH_3(CH_2)_{15}N(Br)(CH_3)_3$, or CTABr, Sigma-Aldrich) was also incorporated at 0.05%wt to stabilize the gas bubbles generated in the fresh GP paste (O_2 from H_2O_2 and H_2 from the Si impurities present in silica fume). The chemical composition of sodium silicate was adjusted and mixed with NaOH pellets, and let to cool down to ambient temperature (see for Table 1 the exact composition of GP foam). CTABr was mixed with the liquid activating sodium silicate solution. Dry MK and silica fume powders are mixed until homogeneity, before the sodium silicate solution is poured on them. The GP paste is mixed using a planetary DAC 400.2 VAC-P Speedmixer (CosSearch GmbH, Germany) mixer. H_2O_2 was incorporated to the mix after the GP paste was homogenized. The fresh GP coating was deposited at constant mass as a few mm layer on a 3 mm thick sandblasted steel plate. The coating is then let to harden and age in a hermetic bag, at ambient temperature, for 7 days. It gives a foamed GP (hereafter called GP foam), which is fully characterized elsewhere[9].

Table 1 : Chemical composition of the components (determined by X ray fluorescence) and composition of GP foam

	Oxide proportion (%wt)				*Component mass (g +/- 0.001)*
	Na_2O	Al_2O_3	SiO_2	H_2O	GP foam
Metakaolin		40.2	54.1		46.949
Silica fume			96.8		28.079
Sodium silicate (betol 39T)	8.3		27.5	64.2	67.402
Sodium hydroxide	77.5			22.5	7.569
H_2O_2	-	-	-		3.002 (2%wt)
CTABr	-	-	-		0.076 (0.05 %wt)
Total mass (g)					153.077

Thermal and microstructural characterization

The heat conductivity of GP foam was measured by the Hot Disk thermal constant analyzer (TPS2500, Sweden) from Thermoconcept (Bordeaux, France). It is based on the transient plane source method. Data are acquired at room temperature. The condition for the heat pulse power and duration is adjusted for each sample to have optimized response parameters, and to ensure measurement reliability.

X ray micro-computed tomography (micro-CT) was performed at the ISIS4D platform (Lille, France). A voxel size of 6.75 µm was used; 800 to 935 images of 514x432 or 500x500 voxels^2 are obtained. To obtain these huge datasets, before quantitative analysis, all images are cropped in a (X, Y) plane so that sample boundaries and exterior are removed. The remaining image volume was 63.8 mm^3 (before fire test) and 61.5 mm^3 (after fire test). The images are filtered and segmented with the ImageJ software [67], in a minimal manner to avoid information loss. The grey level histogram is only spread over the

whole 0–255 available range. Thanks to an excellent phase contrast, thresholding is then performed using the image stack histogram, by selecting the local minimum grey level value between darker pores and lighter solids.

Directional hemispherical reflectance was measured using an integrating sphere-based method. The measurements were performed at 20 °C on a Vertex 70v spectrophotometer (Bruker, Bellerica, MA, USA) equipped with a 75 mm-large, gold-coated integrating sphere (Bruker A562). 128 scans from 350 to 7500 cm^{-1} were performed with a resolution of 4 cm^{-1}, and the results were integrated between 7.5 and 13 µm to determine the emissivity of the sample. The results were interpreted on the Bruker OPUS software (black body emission calculated at 20 °C), also used to run the spectrophotometer.

Burn-through test

The bench-scale burn-through fire test (fully described elsewhere, in[11]) was developed based on two aeronautical certification fire tests: ISO2685:1998(E) and FAR25.856(b):2003. It consists in exposing the samples to a 116 kW/m^2 heat flux, using a propane torch, as illustrated in Figure 1. The steel backside of the sample is coated with a known emissive paint, at $\varepsilon = 0.92$. The sample is then fixed between 10 mm thick insulating panels from FINAL Advanced Materials (Calsil) and attached using four screws. This test, carried out without any ventilation (to avoid the influence of the convection), is divided into two steps. The propane flame is first calibrated for 5 min on the Calsil panels to ensure that the heat flux is constant and equal to 116 kW/m^2 (corresponding to a flame temperature of ~1100°C) (Figure 1-a). It was done using a water-cooled calorimeter from Sequoia named TG1000-1A 'FAA heat flux gage – Fire research type' located in the center of the Calsil plate. Then, the flame is switched onto the sample and the sample is fire exposed for 30 min (Figure 1-b). At the end of the fire test, the sample is cooled down to room temperature. Time/temperature curves were recorded on the backside of the steel plate using an infrared camera.

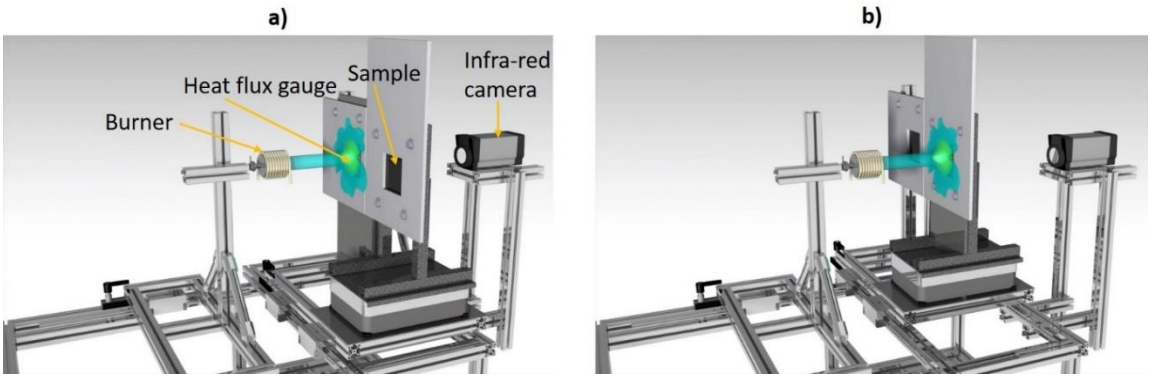

Figure 1. Burn-through test (a) calibration of propane flame and (b) sample fire exposure

Results and discussion

1. *Fire protection after the burn-through test*

The GP foam coated on a steel plate was evaluated after the burn through test and compared to virgin steel. Time/temperature curves were recorded on the backside of the steel plate (center of the plate) and are shown on Figure 1. The temperature reached on the backside of the steel plate is much lower with the GP foam than with the virgin steel. In the steady state, the temperature difference is about 250°C. It is also noteworthy that a plateau can be distinguished at about 100°C for the GP foam. It is assigned to H_2O molecules released from the foam, because of structure changes (amorphization) and almost instantaneous vaporizing. It evidences that GP foam deposited on a steel plate can bring an efficient protection in a severe fire scenario (burn-through conditions at 116 kW/m²). Note that no swelling or expansion was observed during and after the test. The GP foam does not exhibit any intumescence but its behavior looks similar to an already expanded intumescent coating.

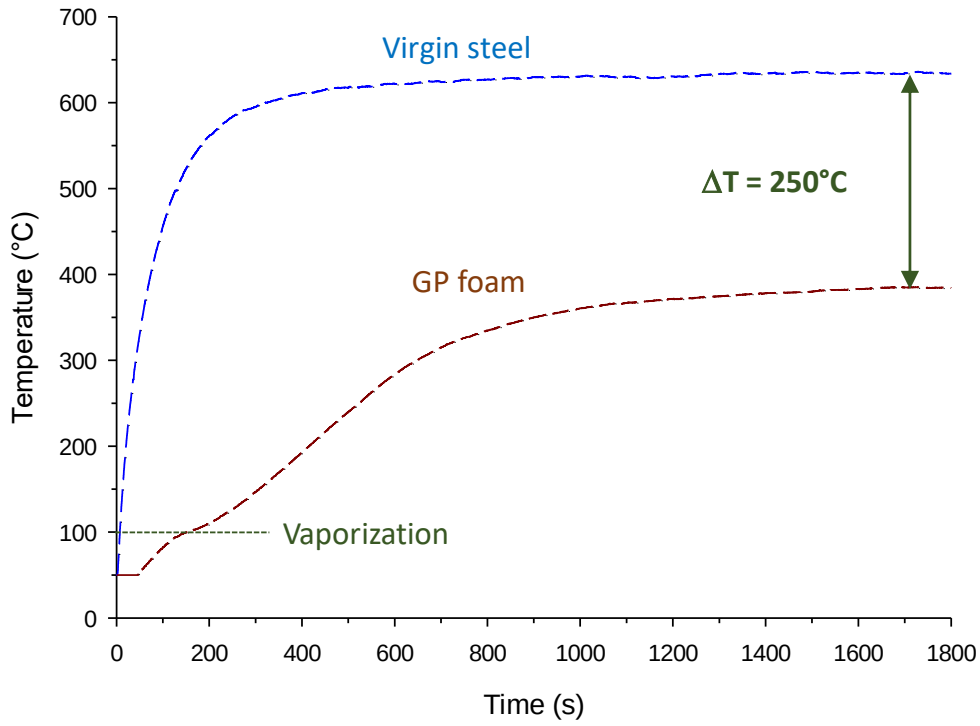

Figure 2. Comparison of the time/temperature curves of a virgin steel plate (in blue) and of a steel plate coated by GP foam (in red) recorded during a burn-through test (temperature measured in the center of the steel plate)

2. *Characterization of GP foam*

Before establishing any numerical model, the material must be characterized to make the model comprehensive and with a physical sense (determination of input data). An example of a 2D X-ray micro-CT image of the structure of GP foam before any fire test is shown in Figure 3. The GP foam exhibits a porous structure of cellular-type, dominated by voids separated by thin GP cement walls. The creation

of voids large in size is explained by the chemical reactions upon synthesis: Si + 4 H_2O -> 2 H_2 + $Si(OH)_4$ (silica fume) and H_2O_2 –> ½ O_2 + H_2O (hydrogen peroxide). Before the GP cement hardens, the bubbles are formed inside the material, and they are stabilized by the surfactant (CTABr), creating a closed porosity structure. Further calculation gave a porosity (ϕ) equal to 81 vol% (before fire test) and 79.6% (after fire test), see more information in our previous paper[9].

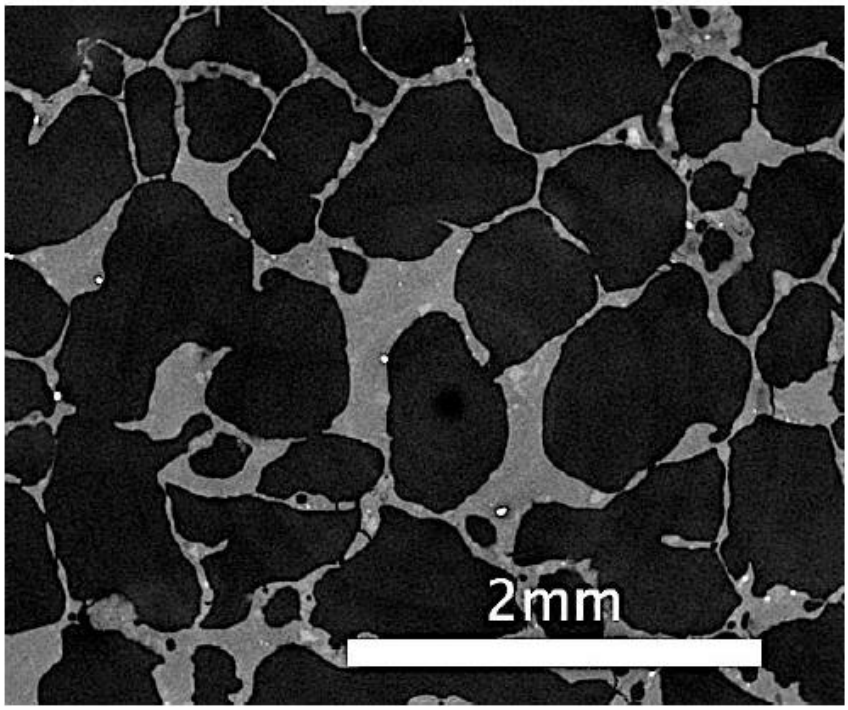

Figure 3. Grey level X ray micro-CT image of the GP foam before fire burn through test; pores are in black and the GP solids are in various grey values

The GP foam is an heterogenous material which can be considered as a porous material constituted by a solid skeleton (geopolymer) and a fluid (air). The thermal conduction in such materials is a complex process involving different types of heat mechanism depending on their structure, pore distribution, chemical composition and so forth. The physical structures assumed in the derivations of the Series and Parallel models are of layers of the components (here there are two components in our materials: fluid and solid) aligned either perpendicular or parallel to the heat flow. According to our previous work[9], it was evidenced that the GP foam followed a parallel model. In the parallel model, there is no heat transfer between the solid skeleton and the fluid because heat transfers in solid and fluid occur at the same time. This model was chosen in the modeling (see next section). Heat conductivity was measured at room temperature and it was found equal to 0.18 W/(m.K). The GP foam is therefore an insulative coating and can reduce heat transfer from the surroundings to the substrate (steel plate here). The heat conductivity of the GP skeleton was also measured, because it is needed in the calculation of the heat conductivity of the GP foam as a function of temperature. After grinding the GP foam, heat conductivity

was measured on the resulting packed powder at a value of 0.55 W/(m.K) (it is assumed that the packing is enough to avoid any significant influence of air between the grains). Those values of heat conductivity are consistent with the work of Duxson[12] reporting the measurement of heat conductivities for metakaolin-based geopolymers. Finally, the emissivity of the GP foam was measured with an integrating sphere at 0.85.

3. *Mathematical formulation*

a) Governing equations

GP foam exhibits a porous structure consisting of a solid and a fluid. The medium is considered isotropic according to the characterizations done in the previous section. In this medium, we assume that there is a local thermal equilibrium so that $T_s = T_f = T$, where T_s and T_f are the temperatures of the solid and fluid phases, respectively. Using those assumptions, the heat diffusion equation through the medium (GP foam) is expressed as follows (Equation 1):

$$(\rho c_p)_m \frac{\partial T}{\partial t} = \nabla \cdot ((k_m + k_{rad})\nabla T) + Q_v \qquad \textbf{Equation 1}$$

where c_p is the heat capacity and ρ the density. The subscript m means the 'medium' because the GP foam is a porous material (combination of air as a fluid (subscript f) and of the GP as a solid (subscript s). k_m is the thermal conductivity of the medium and k_{rad} is the contribution of radiation to thermal conductivity. Q_v denotes the heat source associated with an internal phase transition (here vaporization).

As GP foam is constituted of air and solids then (Equation 2):

$$(\rho c_p)_m = (1-\phi)(\rho c_p)_s + \phi(\rho c_p)_f \qquad \textbf{Equation 2}$$

The heat conductivity in GP foam is calculated according to a parallel model, expressed as (Equation 3):

$$k_m = (1-\phi)(\rho c_p)_s + \phi(\rho c_p)_f \qquad \textbf{Equation 3}$$

k_{rad} is the contribution of radiation to thermal conductivity. For large pores (> 100 µm), the expression of an equivalent thermal conductivity due to radiation across the pore is given through the Loeb's equation[13,14] (Equation 4):

$$k_{rad} = 4\omega d\varepsilon_s \sigma T^3$$ **Equation 4**

where ω is the geometrical factor. According to previous section, the pores are assumed spherical and $\omega = 2/3$. d is the main diameter of the pores; it was measured at 3 mm using X-ray micro-CT and image analysis in a previous work [9]. ε_s is the emissivity of the solid skeleton of the GP foam; it was measured at 0.85 (see previous section).

The thermal effect of vaporization in the pore space (Q_v) is calculated by Equation 5[15]:

$$Q_v = \phi \rho_w \Delta H_v \frac{dS_v}{dt}$$ **Equation 5**

where ΔH_v is the enthalpy change associated to vaporization (2257 J/g), ρ_w is the volumic mass of liquid water and M_w is the molar mass of water (18 g/mol). S_v is vapor saturation, which denotes the volumetric fraction of the void space occupied by the vapor phase. The time derivative, dS_v/dt, specifies the phase transition rate; it is positive because it describes a vaporization. It is a kinetic term which is written like a reaction rate assuming a first order function (Equation 6):

$$\frac{dS_v}{dt} = \kappa\,(1 - S_v)$$ **Equation 6**

where κ is the phase transition rate, which depends formally on the heat flux, the interfacial area and vapor pressure. It cannot be expressed by an Arrhenius law and another approach must be considered. Chen et al.[15] assumed that the phase transition was controlled by the Clapeyron equation and established the following expression (Equation 7):

$$\kappa(\upsilon) = A.tan\left(\frac{\pi}{2}\frac{\upsilon}{\upsilon_v}\right)$$ **Equation 7**

where υ_v is a dimensionless constant, A (in s^{-1}) is a reference transition rate and υ is a state parameter depending on temperature and pressure. Without further experiments and based on the work of Chen et al.[15], υ_v is set at 0.02 and A at 4 s^{-1}.

The GP foam was applied on steel plate and the assembly was embedded in an insulative material (Calsil) (see experimental). In steel and in Calsil, the heat transfer equation simplifies as (Equation 8):

$$\left(\rho c_p\right)_u \frac{\partial T}{\partial t} = \nabla \cdot (k_u \nabla T)$$ **Equation 8**

The subscript u is related to steel and Calsil. All parameters were implemented as a function of temperature using the database of Comsol Multiphysics® (steel) or from our measurements (Calsil).

b) Boundaries

The boundary on the front face corresponds to the impingement of the flame on virgin steel or on GP foam (Figure 4 (a)). The heat flux ($\dot{q}''_{gauge}$) provided by the flame was measured at different positions of the plate. It was found that the applied flux is not uniform across the exposed surface. $\dot{q}''_{gauge}$ is a function of surface coordinates and was implemented in the model. Heat flux $\dot{q}''_{gauge}$ lies between 85 and 116 kW/m² depending on surface coordinates as shown in Figure 4 (b)).

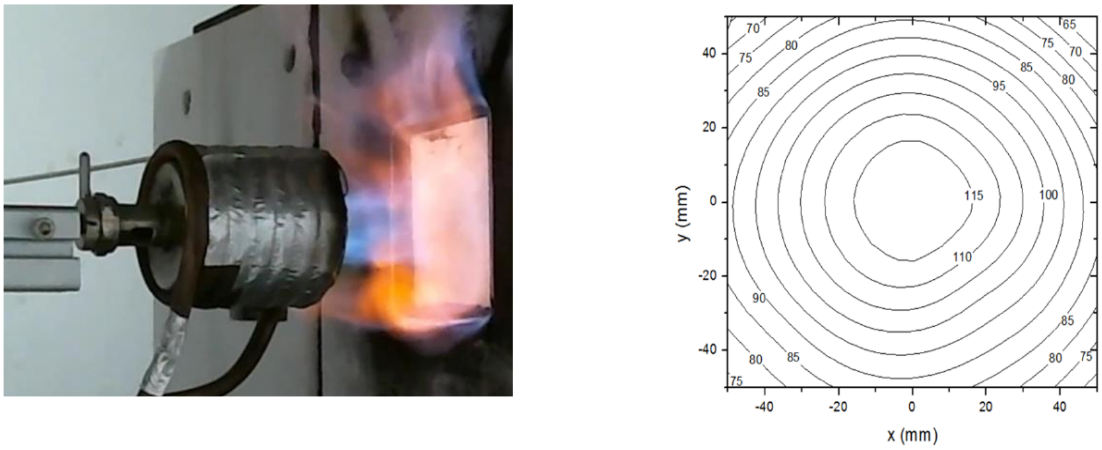

(a) **(b)**

Figure 4: (a) Flame impinging GP foam during burn-through test, and (b) mapping of heat flux at the surface of the plate

If we assume a thermodynamic equilibrium at the surface of the material, absorptivity and emissivity are equal according to the Kirchhoff's law. The net heat flux on the surface of the heat flux gauge, $\dot{q}''_{gauge}$, used to measure the heat flux during the burn-through experiment is then written as (Equation 9):

$$\dot{q}''_{gauge} = \varepsilon_{gauge}\dot{q}''_{flame} + h_{flame\_1}\left(T_{flame} - T_{gauge}\right) - \varepsilon_{gauge}\sigma T^4_{gauge}$$ **Equation 9**

where $\dot{q}''_{flame}$ is the radiant heat flux of the flame, ε_{gauge} is the emissivity of the front surface of the heat flux gauge, σ is the Stefan-Boltzmann constant, h_{flame_1} is the convective heat transfer coefficient,

T_{gauge} is the temperature of the heat flux gauge and T_{flame} is the flame temperature.

Similarly, the net heat flux on the surface of the material (steel or GP foam), $\dot{q}''_{solid}$, is written as (Equation 10):

$$\dot{q}''_{solid} = \varepsilon_{solid}\dot{q}''_{flame} + h_{flame\_2}\left(T_{flame} - T_{solid}\right) - \varepsilon_{solid}\sigma T_{solid}^4 \quad \textbf{Equation 10}$$

where ε_{solid} is the emissivity of the front surface of the material, h_{flame_2} is the convective heat transfer coefficient and T_{solid} is the surface temperature of the material.

The measurement of the heat flux by the gauge was done in a similar way to the experiments on virgin steel and GP foam. Therefore, it is reasonable to assume that $h_{flame\_1} = h_{flame\_2}$. Equation 9 and Equation 10 are then combined together to express $\dot{q}''_{solid}$ and to eliminate $\dot{q}''_{flame}$ (Equation 11) :

$$\dot{q}''_{solid} = \frac{\varepsilon_{solid}}{\varepsilon_{gauge}}\dot{q}''_{gauge} + h_{flame}\left[\left(1 - \frac{\varepsilon_{solid}}{\varepsilon_{gauge}}\right)T_{flame} + \frac{\varepsilon_{solid}}{\varepsilon_{gauge}}T_{gauge} - T_{solid}\right] - \varepsilon_{solid}\sigma\left(T_{solid}^4 - T_{flame}^4\right) \quad \textbf{Equation 11}$$

The boundaries on the other faces are the conventional radiation and convective heat losses (laterally on Calsil and at the back on steel) and are described with Equation 12:

$$-\mathbf{n}\cdot(-k_u\nabla T) = h_{face}(T_{amb} - T_{solid}) - \varepsilon_{solid}\sigma\left(T_{amb}^4 - T_{solid}^4\right) \quad \textbf{Equation 12}$$

where h_{face} is the convective heat transfer coefficient on a face of the assembly (GP foam, Calsil or steel) and $\mathbf{n}$ is the unit vector normal to the surface considered.

c) Meshes

After representing our set-up in 3 dimensions, a 3D mesh is generated as an unstructured mesh with tetrahedral elements containing 7545 domain elements, 3546 boundary elements, 360 edge elements and 25 vertex elements using Comsol Multiphysics® (Figure 5). Different size domains were also evaluated containing 2124, 3636 and 11530 elements; it was found that the best compromise between the computing time and the accuracy was the grid containing 7545 elements (the computation time is 352 s on workstation Xeon® CPU E5-2623 and 64 Gb memory). In the conditions discussed in the next section, the smallest size domain requires 130 s to be solved, while that containing 11530 elements

requires 439 s.

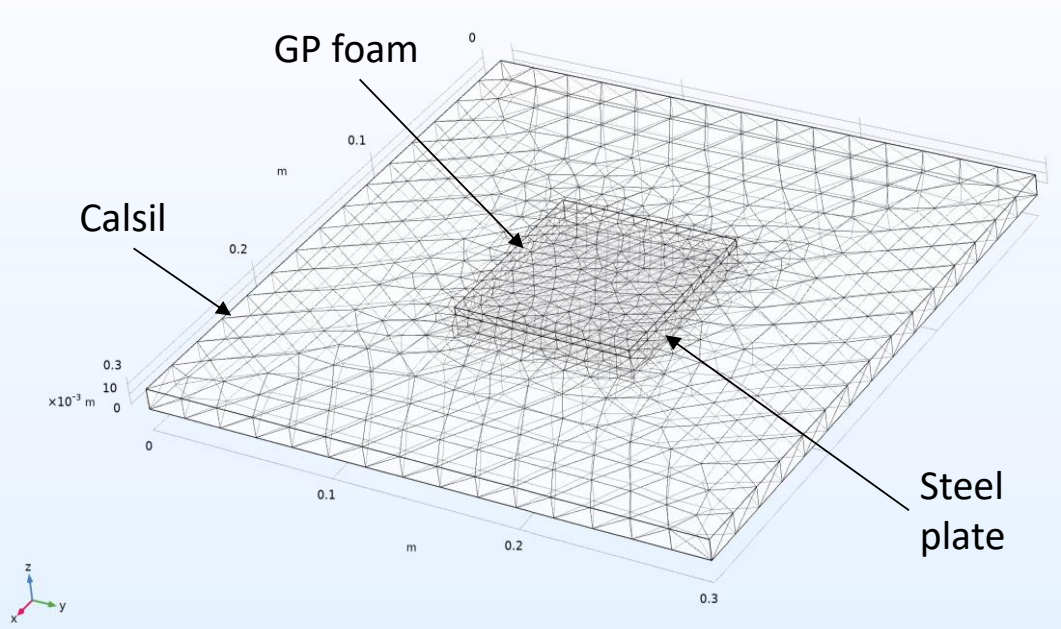

Figure 5: Meshes of the assembly steel plate coated by the GP foam during the burn-through test

4. Numerical simulation

a) Convection coefficient and emissivity

The convection coefficients on the backside and on the side of the assembly were assumed to be 10 W/(m².K) corresponding to a laminar flow on the plate[16]. Equation 11 shows that the convective coefficient h_{flame} is related to the convection created by the flame impinging the surface of the material and the emissivity of steel ($\varepsilon_{solid} = \varepsilon_{steel}$). They were determined by modeling the experiment on the virgin steel plate (its thermal parameters are exactly known as a function of temperature thanks to the database of Comsol Multiphysics®) and by using an inverse method to calculate h_{flame} and ε_{steel}. Here the problem is to reliably determine the values of h_{flame} and ε_{steel}, which provides simulated data that best match measured data, i.e. temperature/time curve of the virgin steel plate in the conditions of the test. The SNOPT code algorithm[17] was used and is implemented in Comsol Multiphysics®. When using SNOPT, the objective function can have any form and any constraints can be applied. The algorithm uses a gradient-based optimization technique to find optimal designs; when the underlying partial differential equation (PDE) is stationary, frequency dependent, or time dependent, analytic sensitivities of the objective function with respect to the control variables can be used. Running this optimization technique gives $h_{flame} = 47.3\ W/(m^2.K)$ and $\varepsilon_{steel} = 0.43$ with an extremely good fit between the simulated and experimental curves when comparing the data measured in the center of the plate (Figure 6). The value of emissivity is consistent with values measured at high temperature for steel and exhibiting low oxidation[18]; the value of the convective coefficient is also consistent with that measured in similar conditions on the burn through test at the reduced scale[19].

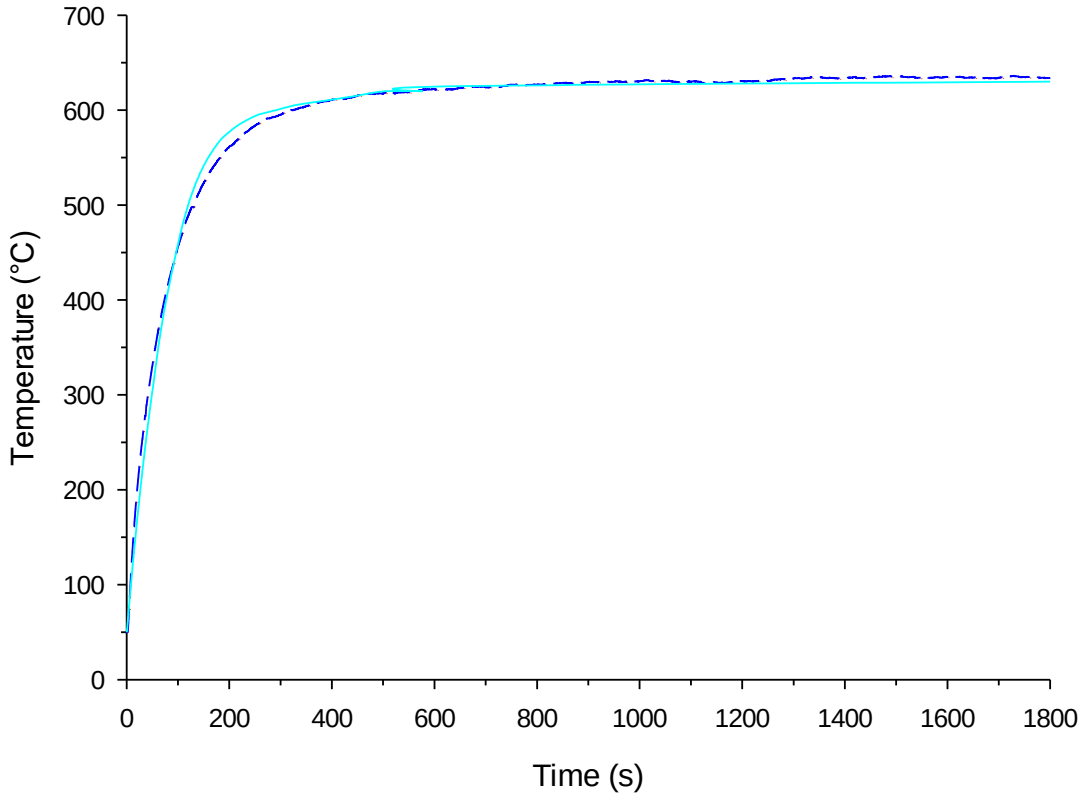

Figure 6: Numerical simulation of the time/temperature curves (dashed: experimental, plain: simulated) of the virgin steel plate (temperature in the center of the plate)

b) Finite element calculation and modeling

The next step of our work is to solve the equations presented in the previous section on a 3-dimensional geometry. The required parameters are the intrinsic properties of the materials (GP foam, insulative material (Calsil and steel) and of the fluid (air)). They may depend on temperature as shown in Table 2. Here, we assume that the emissivity of the GP foam, of Calsil and of steel is constant. The equations presented in the previous section were implemented in the commercial package Comsol Multiphysics® and were solved numerically on a 3-dimensional geometry using finite difference approximations with the prescribed boundaries and with the values of Table 2. The problem to be solved is highly nonlinear and the time-dependent solver was chosen. The algorithm of the time-dependent solver is based on the FEM discretization of the time-dependent PDE problem. The solver is an implicit time-stepping scheme, which implies that it must solve a possibly nonlinear system of equations at each time step. It solves the nonlinear system using Newton iterations, and it then solves the resulting systems with an arbitrary linear system solver. In the time-dependent solver, the time step was specified at 0.01 s over the range 0–1800 s. It is also essential for accuracy to set absolute and relative tolerance parameters for the time-dependent solver. The absolute and relative tolerances, set at 0.1 and 0.01, respectively, control the error in each integration step.

Table 2: Parameters and their associated values used in the computations

Parameter - Unit	Value*
Density, ρ - kg/m^3	ρ_{calsil} = 260 ρ_{steel} = -0.43*T + 7986.5 (300 K < T < 1300 K) ρ_s = 1050
Heat capacity, c_p – J/(kg.K)	c_{p_calsil} = 960 c_{p_steel} = 0.17*T + 431.5 (300 K < T < 1000 K) c_{ps} = 900
Heat conductivity, k – W/(m.K)	k_{calsil} = 10^{-4}*T + 0.21 (300 K < T < 1300 K) k_{steel} = 0.015*T + 9.01 (300 K < T < 1300 K) k_s = 0.55
Emissivity, ε	ε_{calsil} = 0.95 $\varepsilon_{steel\_backside}$ = 0.95 (black painted faces except front face) ε_{steel} = 0.43 (front face) ε_s = 0.85 ε_{gauge} = 0.85
Convective coefficient, h – W/(m².K)	h_{flame} = 47.3 h_{face} = 10
Stefan-Boltzmann constant, σ - W/(m.K^4)	σ = 5.67 10^{-8}
Porosity, ϕ	ϕ = 0.81

**Subscript steel, Calsil and s are related to steel, Calsil and GP skeleton respectively – Steel is stainless steel 310 from Thyssenkrupp and the thermal properties come from the database of Comsol ; the thermal properties of Calsil were given by the supplier and those of GP skeleton were measured.*

The equations were solved with a mesh containing 7545 tetrahedra (the system is numerically stable) and the results are shown in Figure 7. The time evolution of the temperature on the backside of the steel plate coated by the GP foam (measured in the center of the plate on the unexposed side) is well captured by the model. The endothermal effect due to vaporization is also captured. Other temperatures were simulated at different locations on the backside and were compared to experimental temperatures (these temperatures are measured by thermography on the backside of the steel plate). In each case, the comparison between the experimental and the simulated curves is excellent (it is not shown for the sake of brevity). This evidences the reliability of the model.

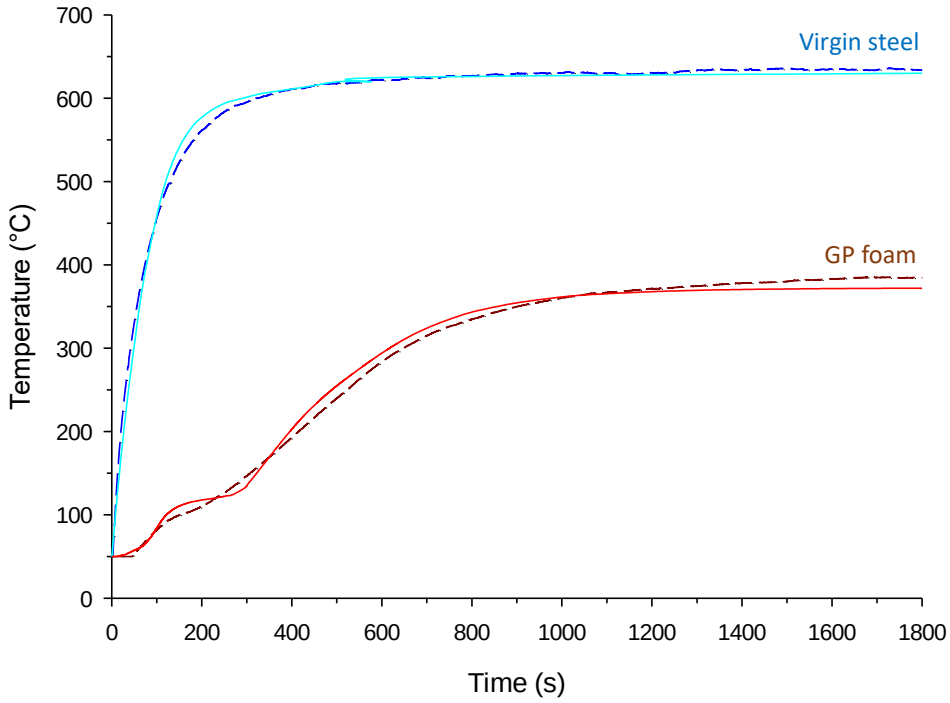

Figure 7: Numerical simulation of the time/temperature curves (dashed: experimental, plain: simulated) of the virgin steel plate and of the steel plate coated by the GP foam (temperature in the center of the plate on the unexposed side)

c) Simulation: parametric study

The model is validated by the experimental results and it gives the opportunity to perform a parametric study on some parameters characterizing the GP foam. The two selected parameters are the emissivity and the porosity of GP foam. For the emissivity, this choice was motivated by one of our previous works evidencing the benefit of depositing a low emissivity layer on top of a polymer[20]. For porosity, it is well known that high porosity materials exhibit low heat conductivity and hence, ensure high insulation. In terms of experiments, porosity can be controlled through geopolymer synthesis.

Figure 8 shows the influence of porosity on the time/temperature curves of GP foam undergoing the burn-through test (temperatures in the center of the plate on the unexposed side). As expected, the higher the porosity, the lower the temperatures. This result does not need specific numerical simulation but it quantifies the influence of porosity: the steady state temperature is about 550°C at 0.1 porosity while it is 360°C at 0.85 porosity and 100°C at 0.95 porosity. The interest of the simulation is that a jump in terms of temperature between 0.85 and 0.9 porosity is evidenced. At $\phi = 0.85$, the temperature rises to the steady state from 300 s while steady state is delayed at 1000 s at $\phi = 0.9$. It strongly suggests to synthesize a GP foam of high porosity to get the highest possible performance.

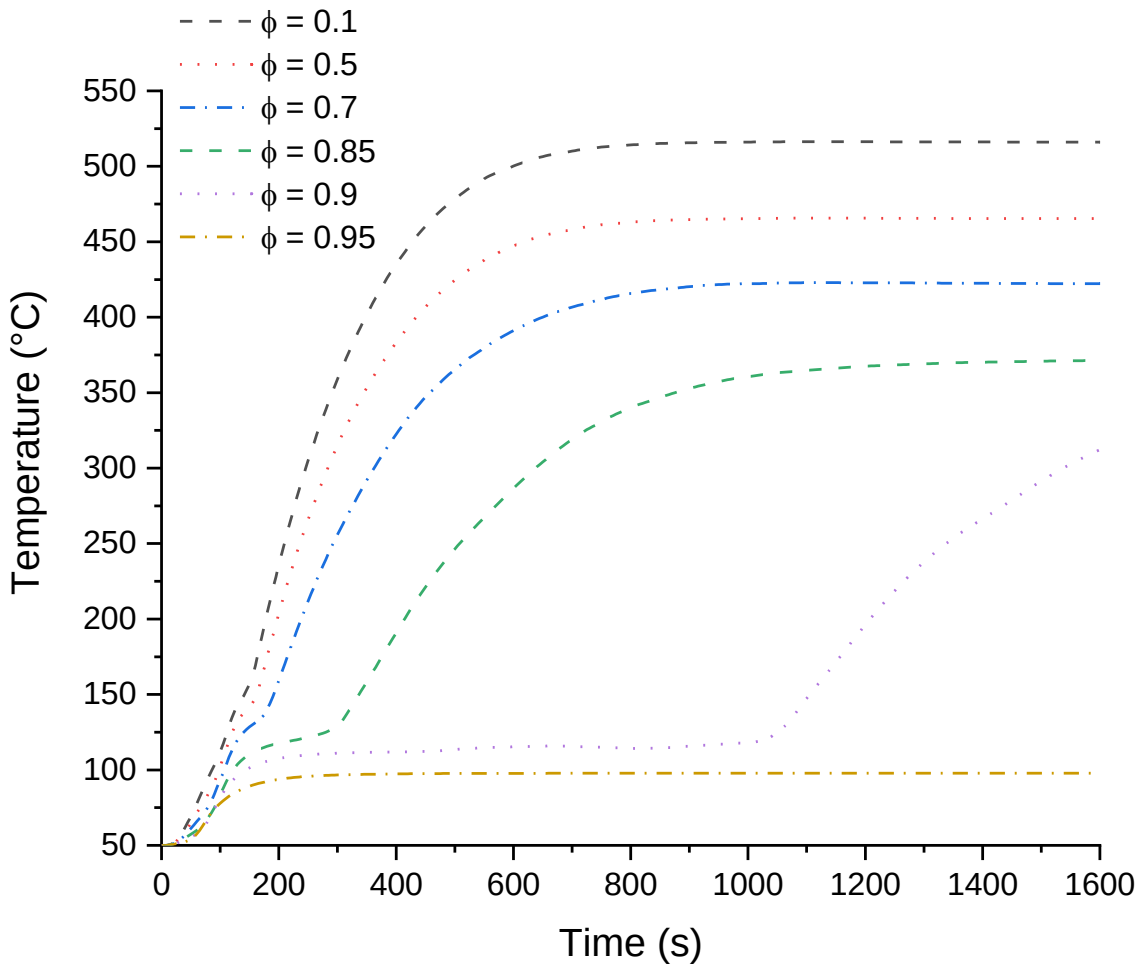

Figure 8: Numerical simulation of the time/temperature curves as a function of porosity ϕ of GP foam (temperatures in the center of the plate on the unexposed side)

The effect of emissivity was also examined. Numerical simulations of time/temperature curves are shown in Figure 9 (temperatures in the center of the plate on the unexposed side). The expected result is that the lower the emissivity at the surface of the GP foam, the lower the temperature on the backside of the material. However, the simulation reveals that an emissivity lower than 0.77 should make the GP foam an efficient fire barrier: the steady state temperature is about 350°C for ε = 0.8 while it is 125°C for ε = 0.75. It suggests that a low emissivity layer could be put at the surface of the GP foam to get a higher performance. The technology is available (see our previous work in[20]) and it should resist to erosion forces delivered by the burner.

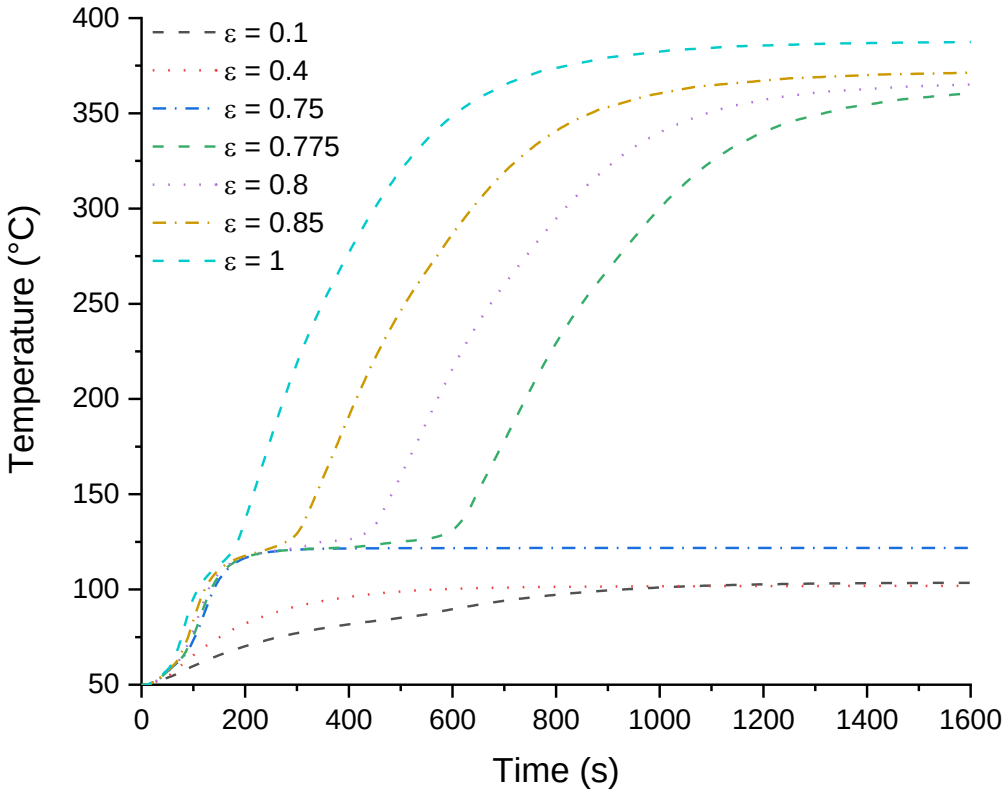

Figure 9: Numerical simulations of the time/temperature curves as a function of emissivity ε of the GP foam (temperatures in the center of the plate on the unexposed side)

The conclusion of this parametric study is that the simulations suggest to make highly porous GP foam combined with a low emissivity layer. Having an emissivity of 0.75 (or lower) is reachable with the technology of thin coating (e.g. Al/Al_2O_3) but to synthesize a GP foam of high porosity (on the order of 0.9) still needs further development.

Conclusion

A GP foam was evaluated in a burn through fire scenario. It was shown experimentally that it is an efficient fire barrier. Further, a numerical model was developed to simulate the fire behavior of the GP foam. It was based on the complete characterization of the GP foam to determine accurate input data for the model. The model captures well the temperature rise, including the endothermal effect due to water vaporization. A parametric study on porosity and emissivity at the surface of the GP foam brings new insights to optimize the performance of the foam. It is shown that a porosity of 90% and an emissivity lower than 0.75 should provide the highest fire performance to GP foam. The fabrication of the optimized GP foam is feasible by using a technology of low emissivity thin coating and by adjusting the synthesis of GP foam to increase its porosity.

Acknowledgement

This work has received funding from the European Research Council (ERC) under the European Union's H2020- the framework programme for Research and Innovation (2014-2020) ERC Grant Advances Agreement N°670747-ERC 2014 AdG/FireBar-Concept for FireBar-Concept project.

References

1. Bourbigot S, Gardelle B, Duquesne S. Intumescent silicone-based coatings for the fire protection of carbon fiber reinforced composites. Paper presented at: 11th IAFSS Symposium2014; Christchuch, New Zealand.
2. Gardelle B, Duquesne S, Vandereecken P, Bourbigot S. Resistance to fire of silicone-based coatings: Fire protection of steel against cellulosic fire. *J Fire Sci.* 2014;32(4):374-387.
3. Duxson P, Provis JL, Lukey GC, Separovic F, Van Deventer JSJ. 29Si NMR study of structural ordering in aluminosilicate geopolymer gels. *Langmuir.* 2005;21(7):3028-3036.
4. Davidovits J. Geopolymers - Inorganic polymeric new materials. *J Therm Anal.* 1991;37(8):1633-1656.
5. Watolla MB, Gluth GJG, Sturm P, Rickard WDA, Krüger S, Schartel B. Intumescent geopolymer-bound coatings for fire protection of steel. *J Ceram Sci Technol.* 2017;8(3):351-364.
6. Sotiriadis K, Guzii SG, Mácová P, Viani A, Dvořák K, Drdácký M. Thermal Behavior of an Intumescent Alkaline Aluminosilicate Composite Material for Fire Protection of Structural Elements. *J Mater Civ Eng.* 2019;31(6).
7. Abdul Rashid MK, Ramli Sulong NH, Alengaram UJ. Fire resistance performance of composite coating with geopolymer-based bio-fillers for lightweight panel application. *J Appl Polym Sci.* 2020;137(47).
8. Shuai Q, Xu Z, Yao Z, et al. Fire resistance of phosphoric acid-based geopolymer foams fabricated from metakaolin and hydrogen peroxide. *Mater Lett.* 2020;263.
9. Sarazin J, Davy CA, Bourbigot S, et al. Flame resistance of geopolymer foam coatings for the fire protection of steel. *Composites Part B: Engineering.* 2021;222:109045.
10. Jaya NA, Yun-Ming L, Cheng-Yong H, Abdullah MMAB, Hussin K. Correlation between pore structure, compressive strength and thermal conductivity of porous metakaolin geopolymer. *Construction and Building Materials.* 2020;247.
11. Tranchard P, Samyn F, Duquesne S, et al. Fire behaviour of carbon fibre epoxy composite for aircraft: Novel test bench and experimental study. *J Fire Sci.* 2015;33(3):247-266.
12. Duxson P, Lukey GC, Van Deventer JSJ. Thermal conductivity of metakaolin geopolymers used as a first approximation for determining gel interconnectivity. *Ind Eng Chem Res.* 2006;45(23):7781-7788.
13. Loeb AL. Thermal Conductivity: VIII, A Theory of Thermal Conductivity of Porous Materials. *J Am Ceram Soc.* 1954;37(2):96-99.
14. Smith DS, Alzina A, Bourret J, et al. Thermal conductivity of porous materials. *J Mater Res.* 2013;28(17):2260-2272.
15. Chen J, Niemeijer AR, Fokker PA. Vaporization of fault water during seismic slip. *J Geophys Res Solid Earth.* 2017;122(6):4237-4276.
16. Bejan A. *Heat Transfer.* Wiley; 1993.

17. Gill PE, Murray W, Saunders MA. SNOPT: An SQP algorithm for large-scale constrained optimization. *SIAM J Optim.* 2002;12(4):979-1006.
18. Zhu C, Hobbs MJ, Masters RC, Rodenburg C, Willmott JR. An accurate device for apparent emissivity characterization in controlled atmospheric conditions up to 1423 K. *IEEE Trans Instrum Meas.* 2020;69(7):4210-4221.
19. Schuhler E, Chaudhary A, Vieille B, Coppalle A. Fire behaviour of composite materials using kerosene burner tests at small-scales. *Fire Safety Journal.* 2021;121.
20. Geoffroy L, Davesne AL, Parent F, et al. Combining Low-Emissivity Thin Coating and 3D-Printed Original Designs for Superior Fire-Protective Performance. *ACS Omega.* 2020:27857-27863.